# SUB-MICRON RESOLUTION OF SECONDARY RADIATION IN LIGA PMMA RESIST EXPOSURE

Aili Ting

MS 9042, Sandia National Laboratories
Livermore, California 94551-0969
925-294-2181, 925-294-1459 (fax)
ating@sandia.gov

Based on the conference paper presented in 2003 SPIE Symposium on Micromachining and Microfabrication Process Technology VIII, 27-30 January 2003, San Jose, California.

## ABSTRACT

Secondary radiation during LIGA PMMA resist exposure adversely affects feature definition, sidewall taper and overall sidewall offset. Additionally, it can degrade the resist adjacent to the substrate, leading to the loss of free-standing features through undercutting during resist development or through mechanical failure of the degraded material. The source of this radiation includes photoelectrons, Auger electrons, fluorescence photons, etc. Sandia's Integrated Tiger Series (ITS), a coupled electron/photon Monte Carlo transport code, was used to compute dose profiles within 1 to 2 microns of the absorber edge and near the interface of the resist with a metallized substrate. The difficulty of sub-micron resolution requirement was overcome by solving a few local problems having carefully designed micron-scale geometries. The results for 10–keV x-ray photons source indicate a 2□/m dose transition region near the absorber edge resulting from PMMA's photoelectrons. This region leads to sidewall offset and to tapered sidewalls following resist development. The results also show a dose boundary layer of around 1 □/m near the substrate interface due to electrons emitted from the substrate metallization layer. The maximum dose at the resist bottom under the absorber can be very high and can lead to feature loss during development. This model was also used to investigate those resist doses resulting from multi-layer substrate.



**Keywords**: LIGA, resist exposure, secondary radiation, undercutting, substrate metalization.


## 1. INTRODUCTION

During LIGA[1] PMMA[2] resist exposure, secondary radiation leads to unwanted doses under the mask absorber. This leads to features having rounded corners and tapered sidewalls. Secondary radiation may also give rise to large doses in masked portions of the PMMA adjacent to the conductive substrate. This may lead to undercutting of features near the substrate, yielding dimensional errors and perhaps the complete loss of some fine features. In addition to undercutting, this secondary radiation near the substrate may degrade the mechanical strength of the PMMA, leading directly to loss of features following complete development. These various concerns are illustrated in Figure 1.

Secondary radiation redistributes the absorbed primary energy. When a photoelectric absorption takes place at a material atomic shell, a photoelectron is emitted, carrying the excess energy that a source photon has above the shell binding energy. Meanwhile, a series of Auger electrons and/or fluorescence photons are emitted during the atom's cascading relaxation. Primary absorption only considers photon energy deposition at its absorption length. As the result, the energy deposition profiles are reasonably uniform in the bulk volume of the resist, but the doses are discontinuous across any material boundary. In fact, photoelectric absorption is eventually realized through electron energy deposition, while any fluorescence photon carrying its unique energy is acting in the same manner as a source photon to produce electrons. Due to the varied directions and very small penetration lengths of electrons, the absorbed energy from a photon is spread around and transits smoothly in a very thin layer near a boundary. Therefore, secondary radiation redistributes the primary absorption dose; it does not superpose on the primary dose.

---

[1] LIGA (**Li**thographie, **G**alvanotormung, **A**bformung in German) means lithography, electroplating, and molding.

[2] PMMA: Polymethyl-methacrylate.

Secondary radiation includes photon secondaries and electron secondaries. Photon secondaries consist of radiation from photoelectrons, Auger electrons, fluorescence x-ray, and recoil electrons (in photon Compton scattering events), while electron secondaries are radiation from electrons and photons resulting from scattering of electrons. In LIGA exposures the energy source is incident x-ray photons, so photon secondaries are the major secondary radiation; electron secondaries are higher order radiation.

With sufficient photon energy, an incident photon absorbed in a material atom K-shell will generate K-fluorescence photons, K-Auger electrons, and photoelectrons. These generated photons and electrons can trigger material atom L-shell events to generate L-fluorescence photons and electrons. This cascading atom relaxation process will continue to the subsequent shells (M-shell and below) until the energy of photon or electron is negligible. Table 1 shows when an incident photon of 10 keV is absorbed in a K-photoelectric event, a photoelectron is emitted and the shell binding energy is distributed into average total energies of all emitted Auger electrons and fluorescence photons following the cascading relaxation process for a few materials of interest. The data of all columns except the last one were taken from EADL Atomic Data Library.[1] Here, probabilities of Auger electrons and fluorescence photons have been included. Thus, the shell binding energy column is equal to the sum of the next three columns: x-ray fluorescence, Auger electrons and local deposition. The primary absorption is simply the incident 10 keV, the sum of the shell binding energy and the photoelectron energy (the second and the last columns), depositing locally, while the secondary radiation absorption (the third to the last columns) deposit to separate places with different penetration lengths and orientations. Note that the local deposition, describing the deposition of the rest energy at the atomic outermost shell at the end of the relaxation process or at the cut-off photon energy, has very small percentage of the binding energy. Unlike Auger electrons and fluorescence photons, photoelectrons carry energies limited only by incident photon energy that is higher than shell binding energy. Auger electrons generally deposit more energy than fluorescence photons do for materials with $Z \geq 30$, since an Auger electron has a greater probability than a fluorescence photon at each atomic shell. For a given source photon energy, K-shell photoelectrons from low-$Z$ materials have stronger energies than from high-$Z$ materials. Thus, for 10–keV source photons, K-photoelectrons deposit much larger energies than Auger electrons except for Cu K-shell absorption, where the large portion of energy is deposited by Auger electrons.

Carbon and oxygen atoms in PMMA have K-shell binding energies well below 1 keV, so their photoelectrons are strong and become the major secondary radiation sources inside the resist. The fluorescence photons and Auger electrons emitted from the PMMA can be ignored because of their relatively small energies (« 1 keV) and small fluorescence yields.

For substrate materials of interest, near the resist bottom boundaries, energy deposited by photoelectrons and/or Auger electrons emitted from the substrate cannot be neglected due to their micron or sub-micron path length. Whether photoelectrons and Auger electrons are important depends on the material. For example, both of them are important for Ti, but Auger electrons are not important for Al, and photoelectrons are not important for Cu. In Table 1, energy deposited by fluorescence photons emitted from Si and Al substrate can be neglected, but that from Cu and Ti may arise in resist bottom provided the substrate is thicker than the penetration lengths. Cu K-fluorescence photons have a penetration length of 18 μm in Cu, but 1.39 mm in PMMA, while Ti K-fluorescence photons have penetration length of 22 μm in Ti, but 0.23 mm in PMMA. Those fluorescence lengths are much longer than the electron penetration lengths at the energy of interest.

Secondary radiation in LIGA resist exposure has been investigated in recent years.[2-10] Experimentally, Pantenburg and Mohr[2] and Zumaque et al[3] have observed 2-10 μm degradation at the top and bottom of resist for tall structures. Pantenburg and Mohr also investigated the correlation between substrate adhesion and absorber height. The simulation work so far has indicated only sub-micron degradation mostly by using varied Monte Carlo methods (MC). Among these simulations, Murata[4-6] presented detailed analysis of his MC results for very thin PMMA film under low photon energies. Feldman and Sun[7] used a one-dimensional model showing a narrow transition region of 0.1 μm across the absorber inside the resist for low photon energy. Feiertag et al[8-9] defined the lateral degradation of about 0.4 μm in PMMA in their MC results as well as from their measurements by using a dissolution limit of 1.8 kJ/cm$^3$. They also computed resist absorption by Ti substrate fluorescence photons. Schmidt et al[10] presented their MC results showing a 1-1.5 μm substrate boundary layer for Cu and Ti substrates attached to a 500□μm resist bottom. Zumaque et al. run a 64 –processor parallel computer system to investigate the tall resist structure (750 μm). Using 5% of the max dose, they defined a lateral degradation at resist bottom of 0.3 μm for a Ti substrate. Their transition region inside the resist was about 2 μm by using 1.5 kJ/cm$^3$ as the dissolution limit. However, when lowering the dissolution limit, for example, a 100 J/cm$^3$ limit, the degradation will be more severe. Running at workstations, Sandia LIGA exposure models have included photon scattering,[11] fluorescence lines [12-13], and photoelectrons,[14] but not yet included Auger electrons or included all photons and electrons together, so a modeling software including all photon/electron secondary radiation sources is preferable to investigate the secondary radiation damage under Sandia's LIGA operation conditions.

Therefore, coupling photon/electron transport is a more accurate way to describe the photoelectric absorption, especially, in the tiny area near the absorber edge inside the resist and near the resist bottom interface. Although this is a challenge for problems of LIGA x-ray exposure owing to the required sub-micron resolution, this difficulty is overcome by solving a few local problems having carefully designed micron-scale geometries using Sandia's ITS radiation transport software (used originally for high energy gamma rays and electrons from 1 keV to 1 GeV and for geometric dimension much greater than that in our problems).[15-16] This software generates all possible events and calculates all energy deposition following an interaction between an incident photon and a material atom, In this way, sub-micron resolution of the dose profiles within 1 to 2 microns of the absorber edge and near the interface of the resist with a metallized substrate were obtained. This model was also used to investigate secondary resist doses resulting from multi-layer substrate's electrons. Such a multi-layer scheme enables the use of low-*Z* metals (aluminum, magnesium, etc.) to provide good electrical conduction and low secondary doses while also providing a good surface metal (titanium, copper, nickel, etc.) for LIGA electrodeposition. We show that the maximum secondary resist dose can be limited by making the surface layer sufficiently thin.

## 2. SAMPLE PROBLEMS AND RESULTS

To gain the fundamental understanding of the secondary radiation, 10 keV source x-rays was chosen in sample problems as the typical source photon energy for it approximates the peak photon energy band incoming to PMMA in LIGA exposure. 5, 15, and 20 keV were also used in some sample

problems for comparison. It would spend weeks to achieve the calculation or need extensive computer resource if the whole synchrotron spectrum was included due to the sizable computing data involved. In all following calculations, 20 batches were used in each case to minimum the statistical uncertainty. The statistical standard errors (SSE) based on the 20 batches were listed in each sample problem. The energy conservation errors ranged from 6 x $10^{-7}$ to 1 x$10^{-2}$.

SAMPLE PROBLEM 1. Primary Versus Secondary Radiation in PMMA Under the Au Absorber Edge (10–keV source photons). This sample problem calculated secondary radiation distribution at the PMMA feature sidewall. The layout was Si (100 μm thick, 12 μm wide) mask substrate, followed by Au absorber (25 μm thick, 3 μm wide), and PMMA resist (500 μm thick, 12 μm wide), as in Figure S1-1. 4.5 x$10^6$ photons were used for photons only transport and 3 x $10^6$ photons were used for coupled photon-electron transport. The calculation completed in four days (maximum SSE 19%).

The absorption dose distribution over PMMA width was calculated through 112 tall but narrow grids (0.1-μm by 480-μm). In Figure S1-2, the smooth dose curve resulted from electron deposition while the jump curve resulted from photon deposition (primary radiation). The energy deposition by PMMA photoelectrons smoothes the transition across the absorber edge, so the exposure accuracy is thus compromised by unwanted doses within a 2-μm transition region around the absorber edge and from the side. This region thickness is just about the continuous-slowing down approximation (CSDA) range[15] of the PMMA electrons at 10 keV.

SAMPLE PROBLEM 2. Doses at Masked PMMA Bottom For Cu-Si Substrate (10–keV source photons). This sample problem calculated PMMA bottom dose boundary layer under mask by the secondary radiation from Cu-Si substrate. The layout was Si (100 μm thick, 16 μm wide), followed by Au (25 μm thick, 8 μm wide), PMMA (500 μm thick, 16 μm wide), Cu (0.5 μm thick, 16 μm wide), and Si (5 μm thick, 16 μm wide), as in Figure S2-1. $10^8$ photons were chosen (maximum SSE 20%). The calculation completed in seven days.

The vertical absorption dose profile at the masked resist bottom was calculated through 30 short but wide fine grids (0.1 μm by 2 μm). Figure S2-2 gives the dose profile in the fine grid zone of Figure S2-1. The two curves have the same trend, although the one with less photon fluctuates more. A 1-μm dose boundary layer from the resist bottom receives significant doses deposited by the substrate electrons that cannot be ignored. At the resist bottom, the dose is about 30 times the average dose (reference value). Hence, the bottom dose may attack the adhesion under the absorber between the resist and the substrate.

SAMPLE PROBLEM 3 (Series). PMMA Bottom Doses by Varied Substrate Materials (5-20 keV source photons). To compare PMMA bottom dose boundary layer for different substrate materials, unmasked PMMA area was chosen to avoid weeks long calculation. Thus, a much shorter height in the open region was adopted, and only two materials (resist and substrate) were selected. Comparison between sample problem 2 and 3 for Cu substrate was an example to show the difference in bottom dose boundary layer between masked and unmasked PMMA. The layout was PMMA (7 μm thick, 11 μm wide), followed by varied substrate material (0.1–5 μm thick, 11 μm wide), as in Figure S3-1. 2–10 x $10^6$ photons were chosen (maximum SSE 4% to 14% for different cases) .

The vertical absorbed dose profile was calculated through 20 short but wide grids (0.1 μm by 5 μm). The twelve calculated cases are for following substrates (10–keV source if not specify): PMMA (5 μm), Cu (5 μm), Ti (5 μm), Al (5 μm), Cu (0.5 μm) , Cu (5 μm, 5 keV), Cu (5 μm, 20 keV), Ti (.1 μm), Ti (.1 μm)-Cu (.4 μm), Ti (.1 μm)-Al (.4 μm), Ti (.01 μm)-Cu(.4 μm), and Ti (.01 μm) Al (.4 μm). These calculations enable us to discuss the influence of substrate material, material thickness, source photon energy, and single or multi-layer substrate, as well as the statistic of the secondary radiation sources.

The results.

(1) Absorption Dose Profiles in Resist Bottom Boundary Layer

Figure S3-2 shows a 2–μm vertical absorption dose profiles from resist bottom. PMMA substrate case was used as a reference (uniform dose throughout), so the resist bottom dose boundary layer that results from the radiation of the substrate electrons can be identified. This layer thickness is around 1 μm at 10 keV (but about 1.5 μm and 0.4 μm for Cu at 20 keV and 5 keV, respectively) that is approximately proportional to the CSDA range of the substrate electrons at the source energy. The exception is the Ti (0.1 μm) case, in which the profile is uniform since the 0.1 μm Ti substrate is too thin to produce any significant photoelectrons and Auger electrons, and the thickness is much less than its electron CSDA range.

(2) Effect of Atomic Numbers of Substrate Material

At 10–keV source, the absorption doses at the resist bottom for 5-μm substrates of Cu, Ti, Al, and PMMA are 20, 14 and 4 times the average open dose due to their descending atomic numbers, as expected.

(3) Advantage of Extremely Thin Ti Top Layer in Multi-layer Substrate.

The cases of 0.01–μm Ti top substrate layer (attached on Cu or Al) make no essential difference in dose profile from the case without Ti, while the cases of 0.1–μm Ti top substrate layer make slight differences. These results suggest thin Ti (thinner than its electron CSDA range at the source energy) can be selected as top surface in multi-layer substrate for designing resist substrate metallization. Such a multi-layer scheme enables the use of low-z metals (such as Al) to provide good electrical conduction and low secondary doses while also providing a good surface metal for LIGA electrodeposition.

(4) Effect of The Cu Substrate's Thickness

In Figure S3-2, the resist bottom dose boundary profiles for all cases with Cu substrate are very similar because the CSDA range of Cu electrons at 10 keV is about 0.5 μm. Therefore, a 5-μm Cu substrate reabsorbs its own secondary radiation inside the substrate at locations 0.5 μm farther from resist bottom, so only the secondary radiation generated at the top 0.5 μm layer of Cu can reach the resist bottom.

(5) Influence of Source Photon Energy

5–, 10–, and 20–keV source energies were compared for a 5–μm Cu substrate. In Figure S3-2, the largest absorption at the resist bottom occurs in 10–keV case, followed by 5–keV and 20–keV cases. The lowest absorption case for 20–keV source is caused by the three times longer CSDA range of Cu electron at 20 keV than at 10 keV, resulting in much less total macroscopic cross section for electrons. On the other hand, no K-shell absorption (only L-shell and below) for Cu will happen at 5 keV, so the absorption is in longer wavelength energy range that produces lesser dose. Although the

average open resist dose at 5–keV source is greater than all cases, it does not result from the substrate but from PMMA itself. The shorter penetration length of 5–keV photons than 10–keV photons in PMMA results in larger average open dose.

STATISTICS OF THE SECONDARY RADIATION SOURCES (from ITS statistic output results)

(1) The Number Ratio of Penetrated Source Photons

Figure S3-3 presents the penetrating source photons ratios from statistic result. The greater the source photons penetration, the lesser the source photons interact with the material atoms, and the lower absorption will result. The lowest 10–keV or 5–keV source photons penetrated ratio of 0.4 for a resist with 5–μm Cu substrate means as many as about 60% source photons interacting with Cu to produce absorption since 10 keV is close to Cu's K-shell binding energy and 5 keV is also not far from Cu's L-shell binding energy, while only 0.5% 10–keV photons interact with PMMA.

The highest 10–keV source photon penetrated cases are 99.5%, 99.4%, 99.2%, 98.9%, and 96.2% for substrates PMMA, Ti (0.01μm)-Al (0.4μm), Ti (0.1μm), Ti (0.1μm)-Al (0.4μm), and Al (5μm), respectively, resulting in only 0.5% to 3.8% source photons interact with resist and substrate atoms. No enough Ti atoms to excite in very thin Ti layer (99% penetrated source photons), and some absorption in Ti (5μm) (77.7% penetrated source photons) were observed. Also note the long 20–keV photon penetration length causes 87% penetrated ratio in Cu (5μm).

(2) Total Energy Deposited by Each Radiation Source for Single 5-μm Substrate at 10–keV Source.

Figure S3-4 shows the total energy deposited by each secondary radiation source for the resist with a 5-μm substrate of Cu, Ti, Al, and PMMA, respectively. Note that the high-order contributions from Compton recoil electrons, Bremstrahlung photons (electron secondaries) and fluorescence photons that originated from electrons are negligibly small.

Contributions from photoelectrons are 89%, 82%, and 58% for PMMA, Al, and Ti substrates, respectively, dominating in all cases except for the Cu substrate (25%) because photoelectrons emitted from Cu are relatively weak (1.1 keV). Photoelectrons emitted from C and O in PMMA are the strongest (10 keV) due to the low K-shell binding energy of C and O (below ITS 1–keV cut-off energy), following by from Al (8.4 keV), and from Ti (5.1 keV).

No Auger electrons present for the PMMA substrate (below 1 keV), while they are the most important radiation source for the Cu substrate (40%), followed by the Ti substrate (30%), and Al substrate (12%) because of their descending K-shell binding energies.

Fluorescence photons that result from source photons contribute 30% energy for the Cu substrate, more important than the photoelectrons because of high K-shell binding energy. However, fluorescence photons contribute only 8% for Ti substrate due to low K-fluorescence yield (about 0.21), and it can be ignored for Al and PMMA substrates.

Contribution from knock-on (electron scattering) is generally small (about 5%) because of the incident photon source, but much greater than that from Compton, Bremstrahlung, and fluorescence originated from electrons. The noticeable contributions from knock-on electrons are from PMMA photoelectrons, which are comparable with that from Auger electrons for Al substrate, and with that from fluorescence photons for Ti substrate.

(3) Total Energy Deposited by Each Radiation Sources for Substrates Containing Cu
Figure S3-5 shows total energy deposited by each radiation source for Cu (5 μm) and Cu (0.5 μm) at 10–keV source, and Cu (5μm) at 5–keV and 20–keV sources. The energy distribution for Cu (5μm) and Cu (0.5μm) at 10–keV source are similar, in which Auger electrons deposit the most (40%), followed by fluorescence (30%), and photoelectrons (25%). However, for varied photon energy sources, the deposited energy percentage by each source can be very different. For 5–keV source, the photoelectrons are dominant, contributing about 95% of the total energy since fluorescence photons and Auger electrons are produced by the L-shells and below (smaller contribution than the knock-on). For 20–keV source, high-energy source photons produce very high-energy photoelectrons (11.1 keV), depositing about 60% of the total energy, followed by Auger electrons (about 18%), fluorescence (about 14%), and knock on contribution (about 8%) induced by strong photoelectrons.

(4). Total Energy Deposited by Each Source for Substrates Containing Ti.
Figure S3-6 shows the total energy deposited by each source for substrates containing Ti at 10–keV source. The substrates are Ti (0.1μm)-Cu (0.4μm), Ti (0.01μm)-Cu (0.4μm), Ti (0.1μm)-Al (0.4μm), and Ti (0.01μm)-Al (0.4μm). Ti (0.1μm) is plotted as a reference.

Comparing with Figure S3-4, the total energy distribution for substrate Ti (0.01μm)-Cu (0.4μm) is similar to that for Cu (0.5μm), and the energy distribution for substrate Ti (0.01μm)-Al (0.4μm) is similar to that for Al (5μm). However, substrate Ti (0.1μm)-Cu (0.4μm) contributes more photoelectrons than substrate Cu (0.5μm), while substrate Ti (0.1μm)-Al (0.4μm) contributes less photoelectrons than substrate Al (5μm). Therefore, a sufficiently thin good surface metal, like a 0.01μm Ti, will not produce extra dose at the resist bottom.

(5) Absorption in the Substrates
Absorption in a metal substrate usually takes a major part of the total deposited energy, which may produce high temperature and induce unwanted effects to the resist. Figure S3-7 shows the absorbed dose in the substrates (top layer and the second layer). As expected, PMMA substrate has no absorption. Cu substrates absorb the most at 10–keV source whether it is a single substrate or the second layer of the substrate. Cu (0.5μm) and Cu (0.4μm) absorb 25% more than Cu (5μm) due to their more interacting photons per volume excluding penetration and escape. On the other hand, less absorption results from high penetration ratios of 20–keV and 5–keV photons, as well as only L-shells and below absorption occurred at 5 keV.

SAMPLE PROBLEM 4-1. Two-Dimensional Calculation of Resist Bottom Doses for Cu-Si Substrate (10–keV source photons). This sample problem calculated two-dimensional PMMA bottom dose boundary layer across the absorber edge. The layout was Au (25μm thick, 4μm wide), followed by PMMA (500μm thick, 11μm wide), Cu (0.5μm thick, 14μm wide), and Si (5μm thick, 14μm wide), as in Figure S4-11. 4 X$10^7$ photons were chosen (maximum SSE 20%).

The two-dimensional absorption dose profile in a rectangular region of 2μm by 1μm at the PMMA bottom with one half zone under the absorber was calculated through 50 fine square grids (0.2μm by 0.2μm), as shown in Figure S4-11.

The results. Figure S4-12 gives a contour plot of two-dimensional doses in the fine grid zone of Figure S4-11. Figure S4-13 gives the dose curves along five horizontal grid lines (from top to bottom

correspond to horizontal grid lines from bottom to top). The average dose line of the open region is also shown, so a data point above this line in Figure S4-13 indicates a dose greater than the average open dose. Under the absorber, a curved triangle region (height 0.8 μm and width 0.5 μm) at the corner having absorption above the average open dose can be identified along with observation from Figure S4-12. The max dose at the masked bottom corner is about 12 times the average open dose, while in the open region the max dose at the bottom corner is about 20 times the average dose (as indicated in previous sample problem).

SAMPLE PROBLEM 4-2. Two-Dimensional Calculation of Resist Bottom Doses for Al-Si Substrate (10–keV source photons). Same layout and fine grid zone as in problem 4-1, this problem has a top Al substrate layer instead of Cu. More photoelectrons generated in Al than Cu, so this calculation needed longer time to complete. 7 X $10^7$ photons were chosen (maximum SSE 20%).

The results. Figure S4-22 presents the dose contour plot of the fine grid zone, in which the bottom corner dose under the absorber is about 2.1 times the average open dose. Comparing with the results in Figure S4-13, the triangular region in which the absorbed doses are above the average open dose is much smaller (about height 0.5 μm and width 0.3 μm), as expected. Figure S4-23 compares the surface plots of the sample problems 4-1 and 4-2 plotted with the same scale. The results show that the doses in the resist for Cu substrate are about five times larger than that for Al substrate, so Al is a better substrate.

SAMPLE PROBLEM 5 (Series). Resist Bottom Doses for Varied Thickness of Ti (0.005–1 μm) in Ti-Al Substrate (5–20 keV source). This sample problem calculated the influence of Ti thickness in the PMMA bottom dose for a Ti-Al substrate. The layout was PMMA (7 μm thick, 11 μm wide), followed by Ti (varied 0.005–1 μm thick, 11 μm wide), Al (0.4 μm thick, 11 μm wide), and optional Si (10 μm thick, 11 μm wide), as in Figure S5-1. The bottom absorption doses were calculated through only two short but wide fine grids (0.1 μm by 5 μm) in the open region under source photon energy of 5, 10, 15, and 20 keV. 3–20 x$10^6$ photons were chosen (maximum SSE 1% to 11% for different cases).

The results. It can be seen in Figure S5-2 that there is a transition region of Ti thickness over which the dose absorbed at the resist bottom increases before the thickness reaches Ti electron CSDA range. 5-keV source photon energy produces the highest resist bottom dose because of the shortest electrons CSDA range, while 20–keV source produces a dose at least 10 times smaller. Besides, Si layer does not deposit anything significant at the resist bottom but only prolong the calculation. Therefore, a very thin Ti layer (less than 0.02 μm) is preferred in order to reduce the unwanted dose at the resist bottom.

## 3. SUMMARY AND DISCUSSION

In the LIGA x-ray photon energy range, the radiation energy deposits through photoelectric absorption. Secondary radiation redistributes the absorbed primary energy through photon secondaries (photoelectrons, Auger electrons, fluorescence photons, recoil electrons) and electron secondaries (products from scattering of electrons). Photon secondaries dominate the radiation while electron secondaries are higher-order radiation. During LIGA PMMA resist exposure, those electrons adversely affect feature definition and can degrade the resist adjacent to the substrate leading to

undercutting or loss of free-standing features during resist development or through mechanical failure of the degraded material. By solving a few local problems having carefully designed micron-scale geometries, Sandia's ITS, a coupled electron/photon Monte Carlo transport code, was used to compute dose profiles due to secondary radiation within 1 to 2 microns of the absorber edge and near the interface of the resist with a metalized substrate.

As expected, the computed results show that the dose profiles are determined mainly by photon secondaries due to incident photon source, while the high-order electron secondaries are generally smaller: 5% to 8% by high energy photoelectrons of PMMA at 10–keV source, as well as by photoelectrons of Cu at 20–keV source (in few cases, this contribution is comparable to that from Auger electrons or fluorescence photons). The results also show that the contributions from Compton recoil electrons and Bremstahlung photons can be mostly ignored (less than 1%).

The computed results indicate a smooth dose transition region near the absorber edge inside the resist resulting from PMMA photoelectrons induced by 10–keV source photons. The thickness of the transition region is about 2 μm, close to the CSDA range of PMMA electrons at 10–keV source. This transition region leads to sidewall offset and tapered sidewalls following resist development. In fact, due to 1–keV cut-off energy, all PMMA photoelectrons have energies of 10 keV (both carbon and oxygen K-shell binding energies are lower than 1 keV). Therefore, photoelectrons emitted from PMMA are the major cause of the dose redistribution inside the resist.

The results also show a dose boundary layer near the substrate interface due to electrons emitted from the substrate metallization layer. The distribution varies continuously from the average dose in the PMMA to the dose at the substrate surface. The thickness of this boundary layer is around 1 μm, proportional to the CSDA range of electrons emitted by the substrate material at 10–keV source when the substrate layer is thick. The maximum dose at the resist bottom under the absorber can be much higher than the average dose of the resist open region. These high doses can lead to feature loss during development. The two-dimensional results show this high doses region is a small curved triangle area. For the Cu substrate, the max dose at the resist bottom under the absorber can be 12 times larger than the average open dose, and the curved triangular area is about 0.3 μm by 0.8 μm, while for the Al substrate, the max dose is about five times smaller, and the triangular area is also much smaller.

Also as expected, the resist bottom dose boundary layer results mostly from photoelectrons and Auger electrons emitted from the substrate. Since fluorescence photons have much longer penetration lengths than electrons have, this deposition reaches far beyond the dose bottom boundary layer unless the substrate is very thick. For example, Cu (5μm) at 10–keV source deposits 30% energy in fluorescence energy, but the penetration length is 18 μm. For the mid-high-*Z* material used such as Cu, at 10–keV source, the Auger electrons (~5.37 keV) is the main radiation sources. However, at 20–keV source, photoelectrons become the main radiation source (~ 11.1 keV). For low-*Z* material used such as Al, photoelectrons (~ 8.4 keV) are the main sources. For a mid-*Z* material such as Ti, both photoelectrons (~ 5.06 keV) and Auger electrons (~ 4 keV) are important sources although more Auger electrons are emitted than photoelectrons.

The radiation dose distributions in the resist transition region and the lateral degradation at the resist bottom for Cu agree qualitatively with the results of Zumaque et al, while the dose distribution on the resist bottom boundary layer for Ti is qualitatively close to that from Schmidt et al.

This model was also used to investigate secondary resist doses resulting from a multi-layer substrate. Such a multi-layer scheme enables the use of low-*Z* metals (aluminum, magnesium, etc.) to provide good electrical conduction and low secondary doses while also providing a good surface metal (titanium, copper, nickel, etc.) for LIGA electrodeposition. We show that the maximum secondary resist dose can be limited by making the surface layer sufficiently thin, i.e., thinner than its electron CSDA range at the source energy.

**ACKNOWLEDGMENTS**

The present work was funded by the Sandia LIGA Technology Maturation Program. Sandia is a multiprogram laboratory operated by Sandia Corporation, a Lockheed Martin Company, for the United States Department of Energy under contract DE-AC04-94AL85000.

The author would like to thank Stewart K. Griffiths for his helpful discussion on selecting sample problems and reviewing the manuscript, Brian C. Franke for his help in using ITS software package, and Dawn Skala for reviewing the manuscript.

**REFERENCES**

1. S. T. Perkins, D. E. Cullen, M. H. Chen, "Table and Graphs of Atomic Subshell and Relaxation Data Derived from the LLNL Evaluated Atomic Data Library (EADL), Z = 1-100," UCRL-50400 Vol 30, October 31, 1991.
2. F. J. Pantenburg and J. Mohr, "Influence of Secondary Effects on the Structure Quality in Deep X-Ray Lithography," *Nuclear Instruments and Methods in Physics Research B* **97**, 551–556, 1995.
3. H. Zumaque, G.A. Kohring, and J. Hormes, "Simulational Studies of Energy Deposition and Secondary Processes in Deep X-Ray Lithography," *J. Micromech. Microeng.* **7**, 79–88, 1997.
4. K. Murata, "Theoretical Studies of Energy Absorption in X-Ray Lithography with Monochromatic X-Rays," *OPTIK* 84, No. 5, 1990.
5. K. Murata, "Theoretical Studies of the Electron Scattering Effect on Developed Pattern Profiles in X-Ray Lithography," *J. Appl. Phys.* **57** (2), January 1985.
6. K. Murata, M. Kotera, K. Nagami, and S. Namba, "Monte Carlo Modeling of the Photo and Auger Electron Production in X-Ray Lithography with Synchrotron Radiation," *IEEE Transactions on Electron Devices*, vol ED-32, No. 9, Sept, 1985.
7. M. Feldman and J. Sun, "Resolution Limits In X-Ray Lithography," *J. Vac. Technol.* **B** 10(6), Nov/Dec 1992.
8. G. Feiertag, W. Ehrfeld, H. Lehr, A. Schmidt, and M. Schmidt, "Accuracy of Structure Transfer in Deep X-Ray Lithography," *Microelectronic Engineering* **35**, 557–560, 1997.
9. G. Feiertag, W. Ehrfeld, H. Lehr, A. Schmidt, and M. Schmidt, "Calculation and Experimental Determination of the Structure Transfer Accuracy in Deep X-Ray Lithography, " *J. Micromech. Microeng.* **7**, 323–331, 1997.

10. A. Schmidt, A. Clifton, W. Ehrfeld, G. Feiertag, H. Lehr, and M. Schmidt, "Investigation of the Adhesive Strength of PMMA Structures on Substrates Obtained by Deep X-Ray Lithography," *Microelectronic Engineering* **30**, 215–218, 1996.
11. A. Ting, "Secondary Radiation in LIGA PMMA Resist Exposures, Part 1: The Influence of X-Ray Scattering, " Sandia Report, SAND2001-8366, May 2001.
12. A. Ting, "Secondary Radiation in LIGA PMMA Resist Exposures, Part 2: The Influence of Fluorescence X Rays, " Memorandum, Sandia, Oct 2001.
13. S. K. Griffiths and A. Ting, "The Influence of X-Ray Fluorescence on LIGA Sidewall Tolerances," *Microsystem Technologies*, v. **8** (#2-3) pp. 120-128, May 2002.
14. S. K. Griffiths, "Fundamental Limitations of LIGA X-ray Lithography," Invited at HARMST 2003 Fifth Biennial Workshop, Monterey, CA, June 15-17, 2003.
15. L. J. Lorence,Jr., R. P. Kensek, J. A. Halbleib, "Adjoint Electron-Photon Transport Monte Carlo Calculations with ITS," *IEEE Transactions on Nuclear Science, vol* **42** *No*. 6, p1895-1901, December 1995.
16. J. A. Halbleib, of Electron Photon Transport Codes –Version 3.0," *IEEE Transactions on Nuclear Science*, *vol* **39** *No*. 4, p1025-1030, August 1992.

Table 1. Distribution of Shell Binding Energies in a 10-keV Photon Absorption Event
(Data from EADL —Evaluated Atomic Data Library of LLNL[1])

| Atomic Shell | Shell Binding Energy | X-ray Fluorescence Lines | | Auger Electrons | | Local Deposition | | Photoelectron Due to a 10 keV Source Photon |
|---|---|---|---|---|---|---|---|---|
| | Eng(keV) | Eng(keV) | % | Eng(keV) | % | Eng(keV) | % | Eng(keV) |
| C(K-) | 0.291 | 0.00047 | 0.16 | 0.262 | 90 | 0.029 | 10 | 9.71 |
| O(K-) | 0.537 | 0.00299 | 0.56 | 0.495 | 92 | 0.039 | 7.3 | 9.46 |
| Al (K-) | 1.549 | 0.055 | 3.5 | 1.46 | 94 | 0.035 | 2 | 8.44 |
| Si (K-) | 1.828 | 0.083 | 4.5 | 1.705 | 93 | 0.040 | 2 | 8.17 |
| Ti (K-) | 4.940 | 0.966 | 19.6 | 3.915 | 79 | 0.060 | 1 | 5.06 |
| Cu (K-) | 8.943 | 3.521 | 39.0 | 5.372 | 60 | 0.050 | 1 | 1.06 |

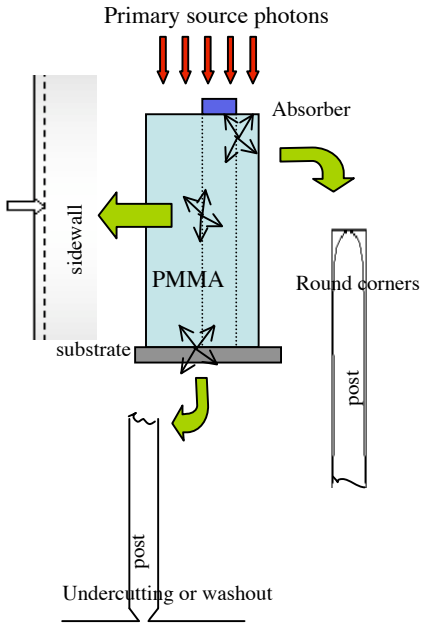


Figure 1. Secondary Radiation

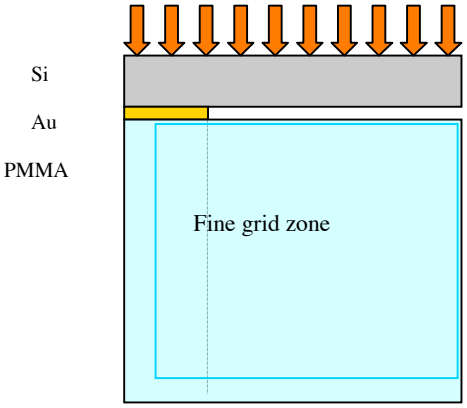


Figure S1-1. Sample Problem 1.

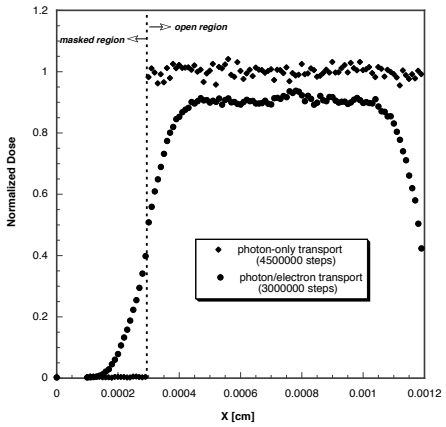


Figure S1-2. Dose Inside PMMA Near Absorber Edge

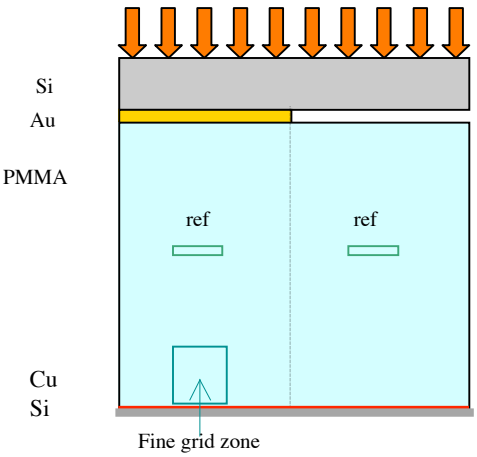


Figure S2-1. Sample Problem 2.

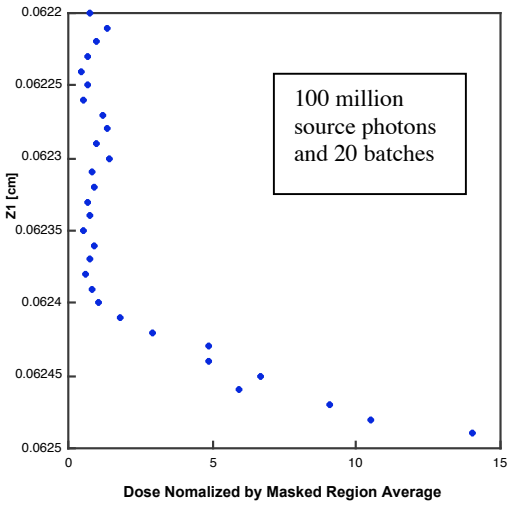


Figure S2-2. Dose near Masked PMMA Bottom by Secondary Radiation from Cu-Si Substrate at

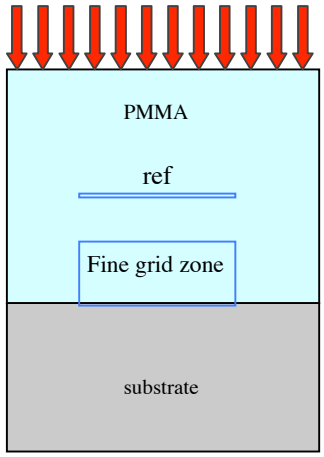


Figure S3-1. Sample Problem 3.

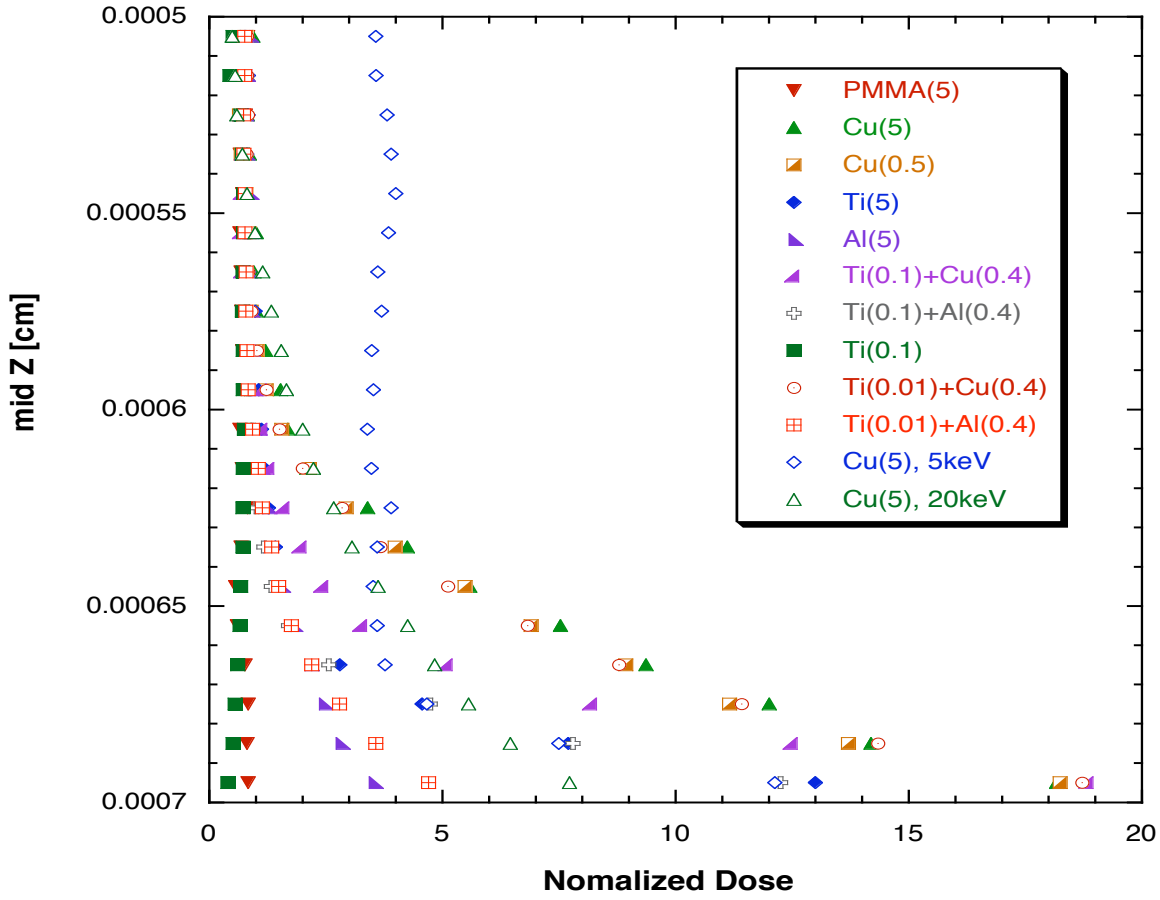


Figure S3-2. Unmasked PMMA Dose Bottom Boundary Layers by Substrate Electrons (10 keV for most single and double layer cases if not specified). Doses are normalized by PMMA bottom dose using PMMA substrate.

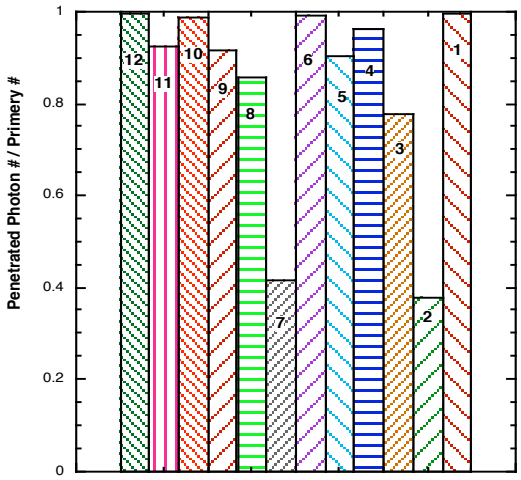


1 PMMA(5)
2 Cu(5)
3 Ti(5)
4 Al(5)
5 Cu(0.5)
6 Ti(0.1)
7 Cu(5) 5 keV
8 Cu(5) 20 keV
9 Ti(0.1)+Cu(0.4)
10 Ti(0.1)+Al(0.4)
11 Ti(0.01)+Cu(0.4)
12 Ti(0.01)+Al(0.4)

Figure S3-3 Source Photon Penetration Number Ratio

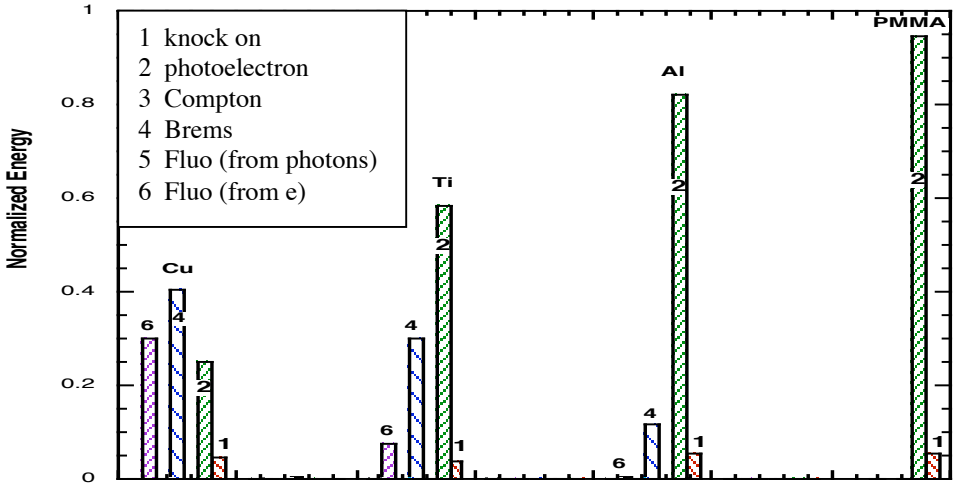


Figure S3-4 Deposited Energy by Secondary Radiation Sources (5-□m Substrate at 10 keV)

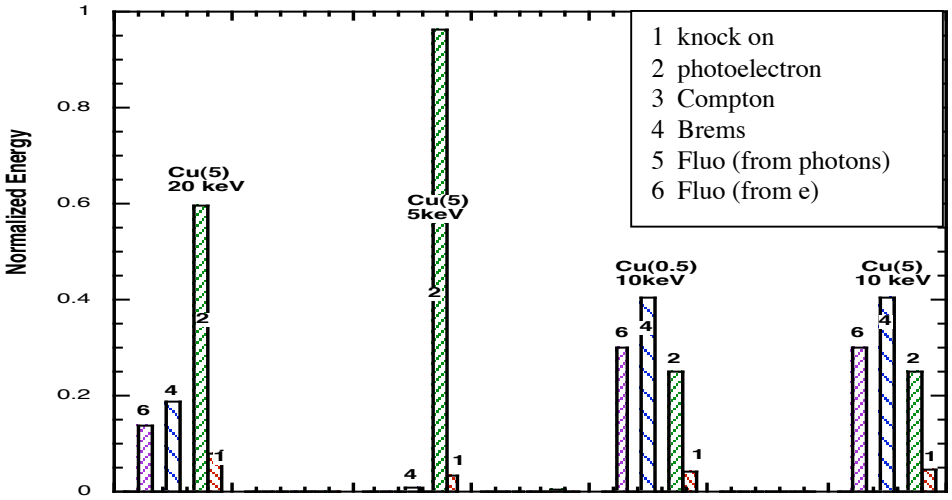


Figure S3-5 Deposited Energy by Secondary Radiation Sources for substrates containing Cu

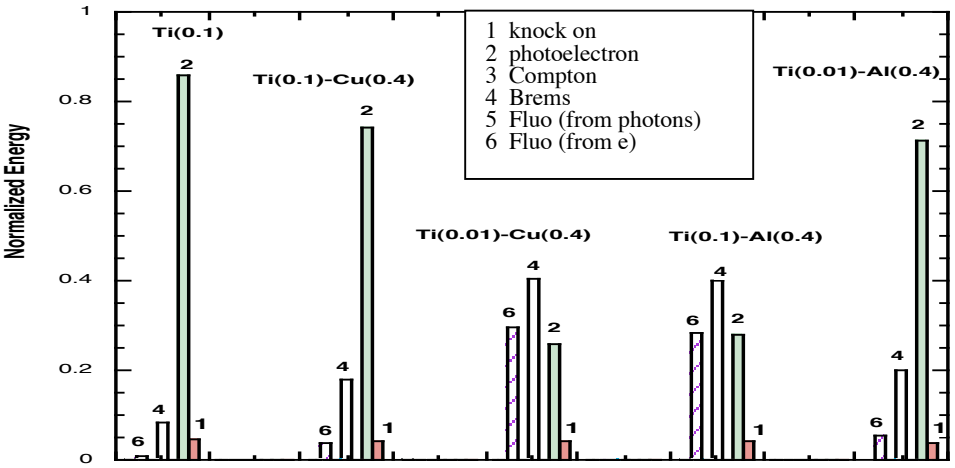


Figure S3-6. Deposited Energy by Secondary Radiation Sources for Substrates Containing Ti

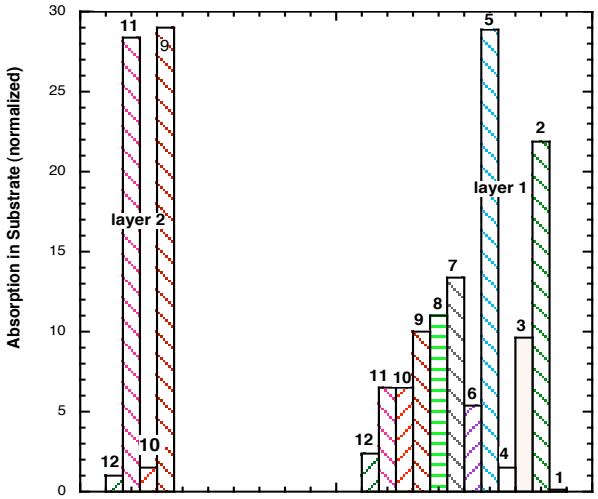


1 PMMA(5)
2 Cu(5)
3 Ti(5)
4 Al(5)
5 Cu(0.5)
6 Ti(0.1)
7 Cu(5) 5 keV
8 Cu(5) 20 keV
9 Ti(0.1)+Cu(0.4)
10 Ti(0.1)+Al(0.4)
11 Ti(0.01)+Cu(0.4)
12 Ti(0.01)+Al(0.4)

Figure S3-7 Absorption in Substrates (layer 1 is the single substrate or the first layer in double-layer substrate, layer 2 is the second layer in double-layer substrate).

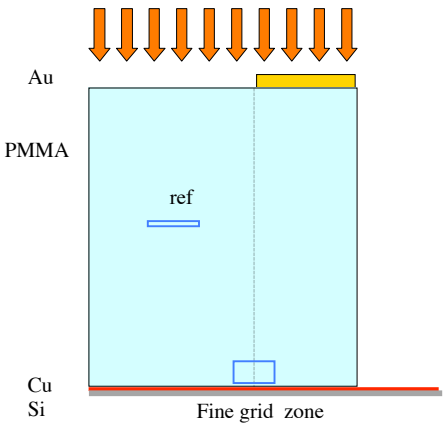


Figure S4-11. Sample Problem 4

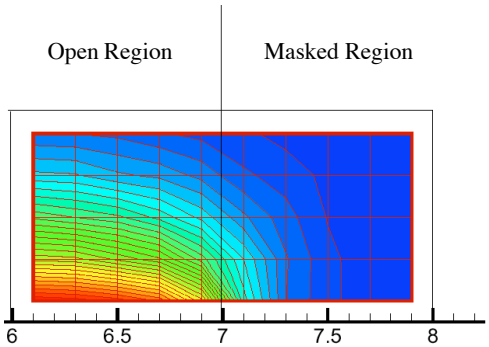


Figure S4-12. Dose Contours at PMMA Bottom (fine grid zone) from Cu Substrate.

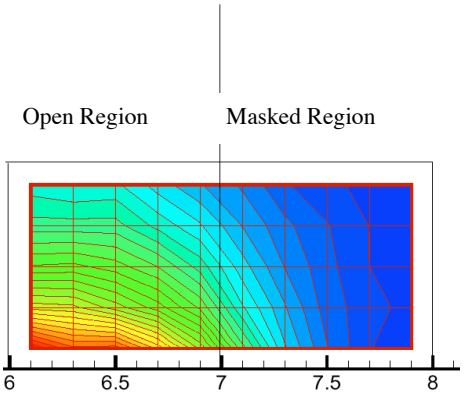


Figure S4-22. Dose Contours at PMMA Bottom (fine grid zone) from Al Substrate

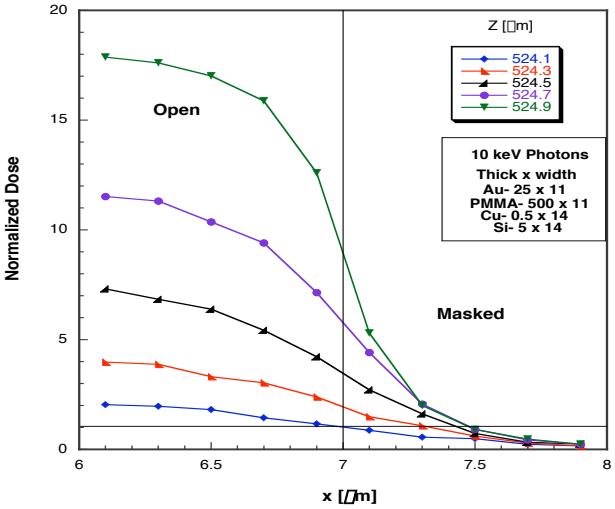


Figure S4-13. Normalized Doses at Horizontal Grid Lines. (normalized by average open dose, top -bottom sequential curves are for bottom-top sequential grid lines)

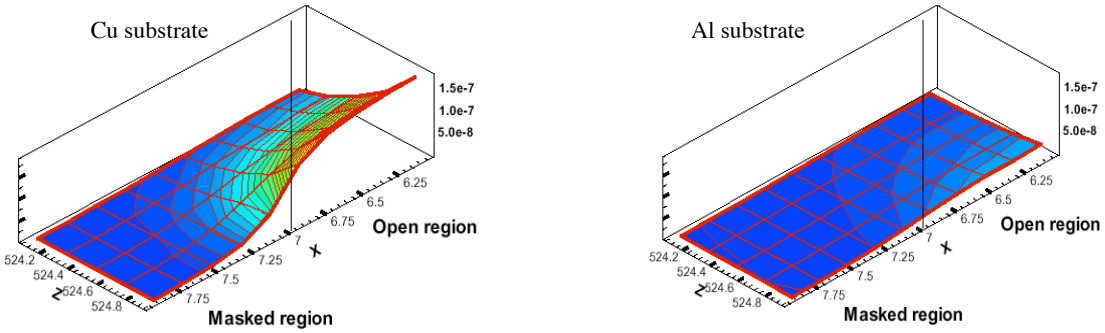


Figure S4-23. Comparison PMMA Bottom Dose Across Absorber Edge for Cu and Al Substrate

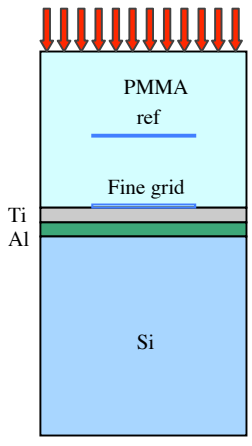


Figure S5-1
Sample Problem 5

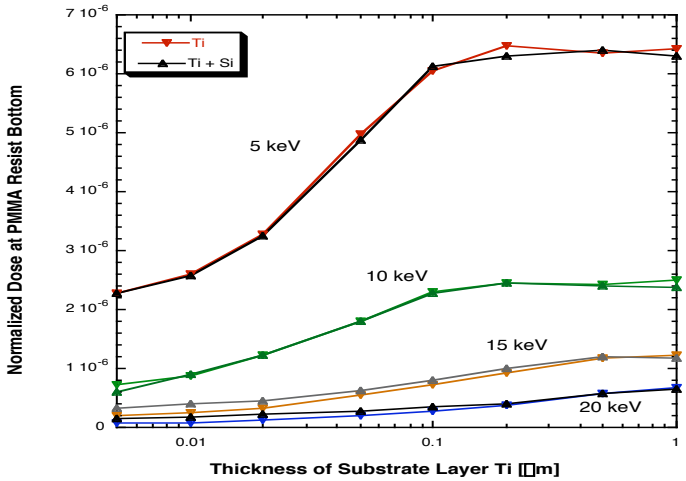


Figure S5-2. PMMA Bottom Dose in Changing Ti Thickness for Ti and Ti-Si Substrates at 5, 10, 15, and 20 keV Sources.